Double magnetic proximity in $Fe/Fe_{0.32}V_{0.68}$ superlattices

H. Palonen,[1,*] F. Magnus,[2] and B. Hjörvarsson[1]
[1]*Department of Physics and Astronomy, Uppsala University, Box 530, SE-75121 Uppsala, Sweden*
[2]*Science Institute, University of Iceland, Dunhaga 3, IS-107 Reykjavik, Iceland*

(Received 2 July 2018; revised manuscript received 21 September 2018; published 12 October 2018)

The conventional magnetic proximity effect and double-proximity effects were studied in a set of fully coherent high-quality $Fe/Fe_{0.32}V_{0.68}$ superlattices. Applying a simple model to the saturation magnetization, it is seen that the magnetic proximity effect is gigantic in magnitude in the alloy—the magnetization is enhanced by 20–450 % and the ordering temperature is enhanced by a factor of 2. The magnitude of the effect can be explained by the large susceptibility of the alloy above its intrinsic ordering temperature. Additionally, a strong dependence of the ordering temperature of single monolayers of Fe on the interlayer distance is observed. The results give insight into new ways of using alloying and large magnetic susceptibility combined with magnetic proximity effects to enhance the functionality of materials that are of interest for spintronic devices.

DOI: 10.1103/PhysRevB.98.144419

I. INTRODUCTION

Surfaces and interfaces become more and more significant as the system dimensions decrease. The interaction between the atoms across an interface, i.e., hybridization of the bands and charge transfer, is responsible for the magnetic proximity effect (MPE), where a magnetization is induced in a nonmagnetic material through proximity to a magnetic material [1]. Additionally, there is a reduction in the ordering temperature in small systems, which is called the finite-size effect [2,3]. A profound understanding of the size and magnitude of these interface effects is essential not only from the fundamental research point of view but also for applications because it alters the behavior of all spintronic devices when scaled down to the nanoscale. For example, the low ordering temperature of (Ga,Mn)As, which is a dilute magnetic semiconductor, can be enhanced by 100% by depositing a layer of Fe on top of it [4]. Thus, the MPE is a possible way to expand the choice of materials for spintronic devices operating at room temperature.

Investigations of finite-size effects are typically not done using self-standing ultrathin films, which means that the measurements are done under conditions in which the MPE is also present. For example, a single monolayer (ML) of bcc Fe is not magnetic on V(100) but is magnetic on Au(100) [5–7]. Consequently, the interplay between MPE and finite-size effects results in a double-proximity effect (DPE). Conceptually it can be understood as a process in which first the short-range correlations in the source induce a magnetization in the surrounding material, which in turn increases the apparent thickness of the source allowing for the long-range order to take place. An example is shown in Fig. 1, where a single ML of Fe is magnetic in an $Fe_{0.32}V_{0.68}$ alloy at temperatures where neither of the components is magnetic on its own. Thus, combining two components that do not exhibit magnetic order can result in ferromagnetism due to a DPE. Here one component is not magnetically ordered because the layer is too thin, the other because it is above its ordering temperature. In the conventional MPE, the high ordering temperature material enhances the ordering temperature of the material with the lower one, but in the DPE the enhancement occurs in both materials.

The purpose of the present work is to investigate the range and magnitude of the proximity effects in a system of two Fe layers separated by a ferromagnetic spacer. The spacer was chosen to be a random bcc alloy of $Fe_{0.32}V_{0.68}$ used above its ordering temperature (≈104 K [8]). Since the superlattice is a combination of very short-range interface effects and long-range itinerant magnetism, it is not trivial to predict the relevant length scale. One would expect that a typical range of the MPE would be the same as the range of the changes in the electronic structure caused by the interface, which has been measured to be less than 5 ML [9,10]. Indeed, in the case of an Fe/V interface, the range of the MPE is confined to about 5 ML [11]. On the other hand, with a highly polarizable medium, e.g., an Fe/Pd interface, the range can be substantially larger, up to 2 nm [12].

In this paper, a strong dependence of the ordering temperature of single monolayers of Fe on the interlayer distance is reported. The huge magnitude of the proximity effects and the role of the susceptibility of the $Fe_{0.32}V_{0.68}$ spacer will be examined by applying a simplified model to explain the measured saturation magnetizations of the samples.

II. EXPERIMENTAL DETAILS

Superlattices with the structure $Fe_{0.32}V_{0.68}(n$ ML)/[Fe(1 ML)/$Fe_{0.32}V_{0.68}(n$ ML)$]_R$ were chosen as a model system for the DPE and long-range exchange interactions. The superlattices were grown on MgO(100) substrates sandwiched between 10-ML-thick V buffer layers and protected with a 5 nm Pd capping layer. The details of the sample layout are

*Author to whom correspondence should be addressed: heikki.palonen@physics.uu.se

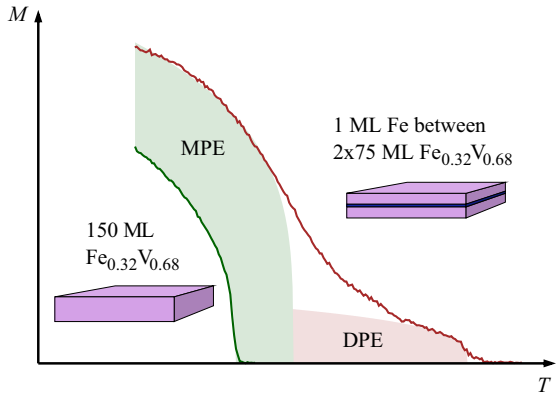

FIG. 1. A schematic of the enhancement in the magnetism of $Fe_{0.32}V_{0.68}$ through magnetic and double proximity effects when adding a single monolayer of Fe.

shown in Fig. 2. The substrates were annealed at 1270 K in 3×10^{-6} Pa for 600 s before growth. For the superlattice samples, the thicknesses of the alloy layer were chosen to be $n = 10$, 15, 20, and 30 and the number of repetitions was chosen to be $R = 12$, 8, 6, and 4, respectively, to keep the total thickness of the film similar. Additionally, reference samples of the alloy (150 ML) and the single Fe layer (75 ML/1 ML/75 ML) were grown. In this paper, we use the notation 1–30, for example, to mean that the bilayer of the superlattice has 1 ML of Fe and 30 ML of the $Fe_{0.32}V_{0.68}$ alloy. The total thickness of the magnetic part of the sample is 22–24 nm for all the samples. Having a total thickness less than 30 nm was seen to be important because then the samples had a fully coherent crystal structure. The samples were grown with direct current magnetron sputtering using cosputtering for the alloy layers. The deposition was done in an ultrahigh-vacuum chamber (base pressure of 5×10^{-8} Pa) on a rotating sample holder kept at 620 K for the superlattice growth and cooled down below 310 K before growing the capping layer. The growth rates were calibrated by growing fully relaxed polycrystalline samples on thermally oxidized silicon substrates. The thickness of the calibration samples was determined with x-ray reflectometry (XRR). The growth rates were intentionally tuned to be low to achieve higher precision and accuracy of growing monolayers (Fe: 0.0118 nm/s, V: 0.0296 nm/s).

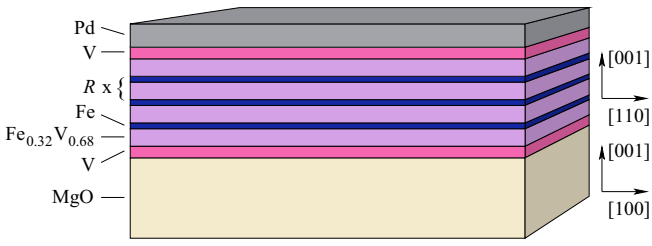

FIG. 2. A schematic of the sample layout. The superlattice stack is begun and ended with the same component, which means that there is always one alloy layer more than there are Fe layers. In the depicted case, the number of repetitions (R) is three. The stack grows 45° rotated in-plane compared to the MgO.

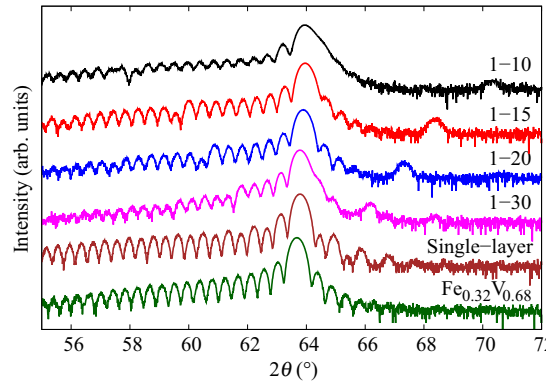

FIG. 3. The measured XRD patterns of the samples that show the (002) main Bragg peak with its Laue oscillations and satellites. The intensity is on a log scale and the curves have been shifted for clarity.

The XRR measurements were done using a Panalytical X'Pert MRD system with a Göbel mirror on the incident side and a parallel plate collimator on the detector side. The x-ray diffraction (XRD) measurements were done on a Panalytical X'Pert MRD system with a hybrid monochromator (Cu $K\alpha 1$) on the incident side and with a Göbel mirror on the detector side. The magnetic characterization was done using the magneto-optical Kerr effect (MOKE) and vibrating sample magnetometry (VSM). The MOKE measurements were done using a 660 nm diode laser operated at 6 mW. The MOKE setup has a pair of Helmholtz coils inside a magnetic shielding, which makes it suitable for measuring extremely soft samples. The VSM measurements were done in a Cryogenic Ltd. superconducting magnetic system in a longitudinal geometry.

III. RESULTS AND DISCUSSION

A. Structural characterization

The quality of the superlattices was established by XRR and XRD. The measured (002) Bragg peaks in diffraction are shown in Fig. 3 and indicate a fully coherent crystal structure for all the samples, as is seen by the high amplitude of the Laue oscillations. Also the satellites are visible but weak, which is to be expected because both the contrast between the layers and the number of repetitions are low. Additionally, the superlattices start and end with the alloy layer, which causes the beating effect of the satellites on the left side of the main peak. The average lattice parameters calculated from the main peak are given in Table I. The lattice parameters show a monotonous decrease when increasing the relative amount of Fe in the samples, which is consistent with the smaller lattice parameter of Fe compared to V. The rocking curve full width at half-maximum of the (002) peaks was measured to be less than 0.06° for all the samples, which also emphasizes the high quality in the context of metallic superlattices.

The contrast between the Fe and alloy layers in XRR is too small to have any Bragg peaks that would contain information on the quality of the layering and interfaces. However, the diffraction data show clear satellites, which confirms the high quality of the layering of the superlattices. The high quality is further supported by the earlier work of our group on

TABLE I. The number of repetitions (R), bilayer thicknesses (λ), the out-of-plane lattice parameters (c), and the ordering temperatures (T_c) of the samples. The sample design of the superlattices is shown in Fig. 2 and for the single-layer and $Fe_{0.32}V_{0.68}$ references in Fig. 1. The total thickness of the magnetic stack is 22–24 nm for all the samples, including the references.

Sample	R	λ (nm)	c (Å)	T_c (K)
1–10	12	1.68(2)	2.908(1)	333.7(2)
1–15	8	2.43(2)	2.909(1)	253.6(3)
1–20	6	3.17(4)	2.911(1)	253.5(4)
1–30	4	4.75(5)	2.916(1)	228.7(7)
Single layer			2.916(1)	226(1)
$Fe_{0.32}V_{0.68}$			2.920(1)	103.1(2)

Fe/V superlattices, which are grown with the same recipe and have contrast to verify the high quality of the layering using XRR [13]. Because the structural results show full coherency, the strain state of the samples is almost perfectly identical. Thus, all the differences in the samples from a magnetic point of view can be attributed to the change in the distance between the Fe layers.

B. Magnetic anisotropy

The average magnetizations of the samples were measured with MOKE and VSM. The anisotropy of the $Fe_{0.32}V_{0.68}$ alloy follows that of a typical bcc ferromagnet, as can be seen in Fig. 4. The easy axis is along [100] and the hard (intermediate) axis is along [110]. The single-monolayer sample is close to isotropic above the T_c of the alloy and follows the same anisotropy as the alloy at low temperatures. Since most of the magnetic moment in the single-layer sample is spread out to the highly polarizable paramagnetic alloy, it makes sense that it is very isotropic. The spread of the moment can be justified by a rough calculation: If the whole measured moment of the single-layer sample at 200 K were only at the Fe monolayer, then each Fe atom would have a moment of $2.6\mu_B$, which is clearly too large. On the other hand, if the moment of each Fe atom were $0.75\mu_B$ (this value will be justified later), then the magnetization would need to be spread across 9 ML to account for the total moment. This already implies that the range of MPE must be at least of the order of nanometers in this system.

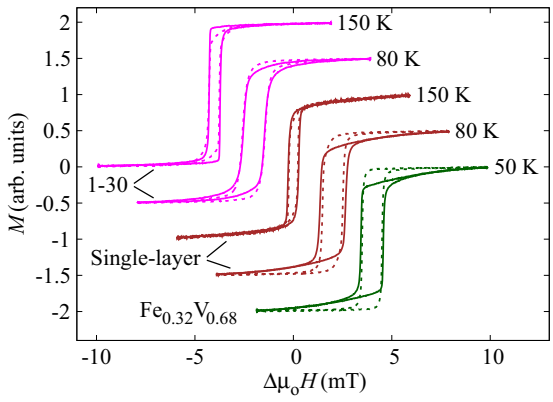

FIG. 4. Examples of the hysteresis loops measured with MOKE. Dashed lines are measured along the [100] and solid lines along the [110] crystalline axis of the superlattice. The curves are shifted for clarity.

The rest of the samples with more than one Fe layer have a magnetic easy axis along the [110] of the bcc structure above the ordering temperature of the alloy while the anisotropy axes are reversed to the [100] easy axis below the ordering temperature, as can be seen in Fig. 4. The deviation from near isotropy with multiple layers could be caused by neighboring layers cutting off the polarization cloud in the alloy, which would then give more relative weight to the monolayer leading to more pronounced anisotropy. That would imply that the intrinsic easy axis of the Fe monolayer is the [110] direction. It is also possible that the anisotropy is induced by atomic steps on the substrate [14]. However, the observed change in anisotropy is consistent over all the superlattice samples, which suggests that it is not induced by the substrate. Comparing the anisotropies with previous work done on Fe/V superlattices shows similar behavior: 4 ML of Fe have an easy axis along [100] but with indications that the interfaces are favoring the [110] direction [15]. 3 ML of Fe are completely isotropic [16]. Thus, a reorientation of the easy axis when decreasing the thickness of the Fe layer is consistent with previous work.

C. Spontaneous magnetization

A full hysteresis loop was measured at each temperature to determine the remanent magnetization, M_{rem}. The MOKE results were then fitted with the power law

$$M_{rem} \sim (1 - T/T_c)^{\beta}, \tag{1}$$

where T is the temperature, T_c is the ordering temperature, and β is an effective exponent. The ordering temperatures extracted from the fits are given in Table I and the power-law fits are shown in the inset of Fig. 5. In this case, the exponents have to be treated as effective ones because the system is not homogeneous, just like in the Fe/Pd system [12]. The effective exponents are almost equal within the errors for all the samples having values between 0.31 and 0.38. Drawing any conclusions about the spatial dimensionality from these values would be incorrect because of the hybrid nature of the system. However, it can be concluded that all the samples behave in an almost identical way near the transition. The similarity can be explained by the fact that near the transition all the magnetization is localized into the vicinity of the Fe monolayers that are identical in the local picture in all the samples.

The remanent magnetization measured along the high-temperature easy axis [110] is shown in Fig. 5. Comparing the alloy reference and the sample with a single Fe layer in the middle of the alloy shows two dramatic effects. First, the DPE increases the ordering temperature by more than a factor of 2, which gives rise to a temperature range between approximately 140 and 240 K, where there is a magnetization in a region close to the Fe layer. Secondly, there is an inflection point at approximately 140 K below which the whole alloy becomes magnetic, and this is also enhanced above the intrinsic ordering temperature of the alloy due to the MPE. These

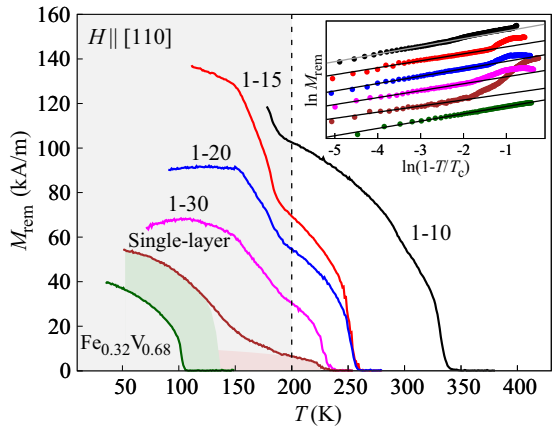

FIG. 5. The remanent magnetization of the samples with the field applied along the [110] direction. The curves were measured with the MOKE setup but have been scaled to absolute units by correlating the saturation values between VSM and MOKE hysteresis loops. The curves are cut off at low temperatures where the applied field in MOKE was not high enough to saturate the sample. The green and brown areas denote the contributions of the MPE and DPE, respectively, as explained in the text. The grayed area marks the range where the temperature dependence of the source is flat enough to allow us to compare the samples approximating them to have similar source strength. Inset: the fits of Eq. (1) to the remanent magnetizations. The curves are shifted for clarity but are in the same order of increasing moment as the curves in the main figure.

two effects are emphasized for the single-Fe-layer sample by the colored areas in Fig. 5. In the superlattice samples, the inflection point is enhanced further up to almost 200 K. Thus, the ordinary MPE in this system is enhancing the T_c of the alloy by a factor of 2. The DPE in the superlattices has a strong dependence on the distance between the Fe layers, which is seen in the enhancement of the ordering temperature of the source by 48% (12%) where the source layers are interacting across a 10-ML-thick (20-ML-thick) paramagnetic spacer, compared to the single Fe layer sample.

All the superlattice samples have a ferromagnetic alignment between the Fe layers. Considering that the structure is ferromagnetic through a connected network of Fe atoms, we can conclude that the coupling between the layers is a direct exchange interaction.

D. Model for the magnetization profile

In contrast with a normal MPE case, where only the induced magnetization is looked for, now the strength of the source is also unknown. However, indirect information about the magnetization of the individual layers can be extracted by looking at how the saturation magnetization evolves when the relative contributions to the magnetization change with different bilayer thicknesses. For this purpose, a simple model for the measured saturation magnetization will now be considered. Comparing the samples with different bilayer thicknesses implicitly assumes that they have similar source strength at that temperature. Thus, the analysis is limited to below 200 K shown by the gray color in Fig. 5 where the temperature dependence of the source is fairly flat.

The average saturation magnetization, M_{sat}, of the bilayer is given by the weighted average of the two sublayers, and it can be written as

$$M_{sat} = L_\delta (M_\delta - M_a)\frac{1}{\lambda} + M_a, \tag{2}$$

where M_a is the average magnetization in the alloy layer, M_δ is the average magnetization of the source layer, L_δ is the thickness of the source, and λ is the bilayer thickness. Consider two different temperature regimes, above and below the intrinsic ordering temperature of the alloy layer. At low temperatures, the alloy is magnetic and the MPE in it is just a small correction to the total moment of the layer. There the magnetization profile in the alloy can be modeled as a constant value. At high temperatures, the alloy is paramagnetic with a large susceptibility; there the profile will decrease exponentially from the source.

Similar to Ref. [11], the profile is expressed as

$$M_a'(z) = C M_\delta \left[\exp\left(-\frac{z}{b\chi}\right) + \exp\left(-\frac{\lambda - L_\delta - z}{b\chi}\right)\right], \tag{3}$$

where b is a temperature-independent fitting parameter while the temperature dependence is contained in the susceptibility χ. There is a discontinuity in the magnetization in the model at the boundary between the layers. This should correspond to the position where the coordination of each Fe atom changes the most, which is 1 ML away from the Fe layer. Note that in a bcc (001) monolayer, all the nearest neighbors are outside the layer. Thus, L_δ is fixed to the value 0.44 nm (3 ML). Assuming that the magnetization drops by a factor of A at the discontinuity, then the boundary condition for Eq. (3) becomes $M_a'(0) = AM_\delta$, which gives

$$C = \left[1 + \exp\left(-\frac{\lambda - L_\delta}{b\chi}\right)\right]^{-1} A. \tag{4}$$

The average magnetization in the alloy layer follows by integrating Eq. (3), which leads to

$$M_a = AM_\delta \frac{2b\chi}{\lambda - L_\delta} \tanh\left(\frac{\lambda - L_\delta}{2b\chi}\right), \tag{5}$$

which is then used in Eq. (2) at temperatures above the intrinsic ordering temperature of the alloy layer. The concepts related to this model and its equations are schematically shown in Fig. 6. This model will be used to fit the saturation magnetizations using Eq. (2) with either a constant M_a ($T < T_c$) or with M_a given by Eq. (5) ($T > T_c$), which will give additional information on how the measured average magnetization is distributed inside each bilayer.

The model is applied here to all the temperatures simultaneously with the following assumptions and fitting parameters: Below the intrinsic ordering temperature of the alloy, M_δ is held constant at a value that is fitted and M_a is fitted as an independent parameter for each temperature. Above, M_δ is assumed to decrease following Eq. (1) with exponent 0.125 and with the ordering temperature of the single-layer sample; M_a is given by Eq. (5) using A and b as fitting parameters. In other words, the temperature dependence of the source is

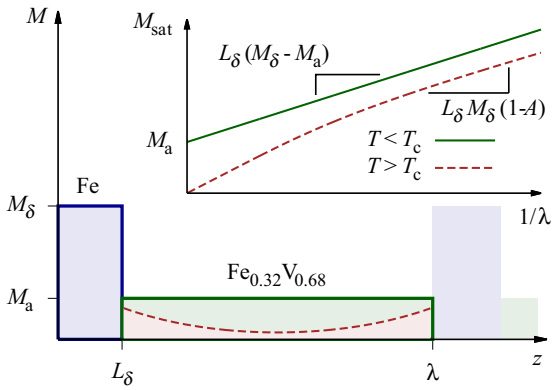

FIG. 6. A schematic of the model for the saturation magnetization profile within a single bilayer. Below T_c of the alloy reference, the profile is modeled as constant (solid line) and above as the exponential given by Eq. (3) shown by the dashed curve. The inset shows how M_{sat} changes with different bilayer thicknesses according to the model. The curves in the inset show Eq. (2), where M_a is either constant (solid line) or given by Eq. (5) (dashed line).

modeled as a two-dimensional (2D) Ising system. For χ the experimental values of the reference alloy are used.

The measured saturation magnetizations and the corresponding fits of the model are shown in Fig. 7, where it can be seen that the model agrees quite well with the experimental values. The resulting fitting parameter values are shown in Table II. The strength of the source is about half of the bulk Fe value, which is quite a lot considering that without the DPE the source layer would not be magnetic at all. Comparing the alloy layer moment with the moment of the reference alloy, it can be concluded that the MPE is enhancing the *average* moment of the alloy by 20–450 % from low temperature to near ordering temperature. Since the experimental data are linear at 2–100 K (Fig. 7) and the value of that line at infinite λ depends only on M_a (Fig. 6), it follows that the values of enhancement are independent of the choice of L_δ. Thus, the enhancement is caused by a very long-range MPE throughout

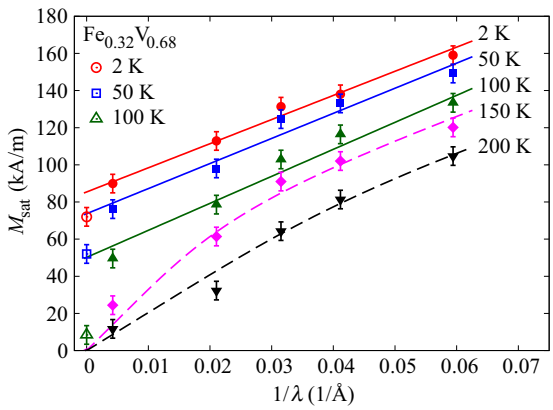

FIG. 7. A fit of the model given by Eq. (2), where M_a is either constant (solid lines) or given by Eq. (5) (dashed lines), to the measured saturation magnetizations shown as points. The saturation magnetization of the $Fe_{0.32}V_{0.68}$ reference alloy is shown by the open symbols on the left.

TABLE II. Fit results from the model for the moments of the individual layers inside the bilayer. Parameters marked with ∧ were constrained to have the same value as at the temperature above during the fit. M_{ref} values were measured from the $Fe_{0.32}V_{0.68}$ reference alloy sample.

T (K)	M_{ref} (μ_B)[a]	M_δ (μ_B)[a]	M_a (μ_B)[a]	A	b (nm)
2	0.31(2)	0.98(3)	0.37(1)		
50	0.23(2)	∧	0.32(1)		
100	0.04(2)	∧	0.22(1)		
150		0.85(3)[b]	0.16(4)[c]	0.16(2)	13(3)
200		0.75(3)[b]	0.08(2)[c]	∧	∧

[a]Calculated per Fe atom assuming a vanishing moment for V.
[b]Calculated from $M_\delta(2\,K)$ using Eq. (1) assuming 2D Ising system with $T_c = 226$ K.
[c]Calculated from A and b using Eq. (5) for the 1–30 sample.

the alloy layer thickness and not by local interface effects that would be lifting the average up. Above the intrinsic ordering temperature of the alloy, the local interface effects are much more pronounced. The characteristic length scale ($b\chi$) of the exponential profile at 150 K is 1.7 nm (12 ML), which is quite long in the context of MPE, but the effect is not as gigantic in range as it is in magnitude. For comparison, a range of MPE longer than 5 nm has been achieved in amorphous systems [17].

IV. CONCLUSIONS

In this work, a set of fully coherent high-quality Fe/$Fe_{0.32}V_{0.68}$ superlattices was grown to study the double-proximity effect and the long-range exchange interactions between the Fe layers over different distances. The double-proximity effect causes a single layer of Fe, which on its own would be nonmagnetic, to become ferromagnetic. Furthermore, the long-range exchange interactions enhance the double-proximity effect, i.e., the ordering temperature of the source, by 48% (12%) across 1.5 nm (3 nm). The ordinary magnetic proximity effect enhances the ordering temperature of the $Fe_{0.32}V_{0.68}$ alloy by 40–100 %. By applying a simple model to the saturation magnetization, it was shown that the magnetic proximity effect has a gigantic magnitude in the alloy—the magnetization is enhanced by 20–450 %. The model also confirms that the huge double-proximity effects can be explained by the large susceptibility of the alloy above its intrinsic ordering temperature. The results of this work provide insight into possible new ways of using alloying and large magnetic susceptibility combined with magnetic proximity effects to enhance the functionality of materials that are of interest for spintronic devices.

ACKNOWLEDGMENTS

F.M. acknowledges funding from the Icelandic Centre for Research (Grant No. 174271-051). H.P. wishes to thank Giuseppe Muscas for fruitful discussions.

[1] P. K. Manna and S. M. Yusuf, Phys. Rep. **535**, 61 (2014).
[2] G. A. T. Allan, Phys. Rev. B **1**, 352 (1970).
[3] F. Huang, M. T. Kief, G. J. Mankey, and R. F. Willis, Phys. Rev. B **49**, 3962 (1994).
[4] C. Song, M. Sperl, M. Utz, M. Ciorga, G. Woltersdorf, D. Schuh, D. Bougeard, C. H. Back, and D. Weiss, Phys. Rev. Lett. **107**, 056601 (2011).
[5] S. Mirbt, I. A. Abrikosov, B. Johansson, and H. L. Skriver, Phys. Rev. B **55**, 67 (1997).
[6] D. Labergerie, K. Westerholt, H. Zabel, and B. Hjörvarsson, J. Magn. Magn. Mater. **225**, 373 (2001).
[7] W. Dürr, M. Taborelli, O. Paul, R. Germar, W. Gudat, D. Pescia, and M. Landolt, Phys. Rev. Lett. **62**, 206 (1989).
[8] A. Mustaffa and D. A. Read, J. Magn. Magn. Mater. **5**, 349 (1977).
[9] P. Srivastava, N. Haack, H. Wende, R. Chauvistré, and K. Baberschke, Phys. Rev. B **56**, R4398 (1997).
[10] S. S. Dhesi, H. A. Dürr, G. van der Laan, E. Dudzik, and N. B. Brookes, Phys. Rev. B **60**, 12852 (1999).
[11] M. A. Tomaz, W. J. Antel Jr., W. L. O'Brien, and G. R. Harp, J. Phys.: Condens. Matter **9**, L179 (1997).
[12] T. P. A. Hase, M. S. Brewer, U. B. Arnalds, M. Ahlberg, V. Kapaklis, M. Björck, L. Bouchenoire, P. Thompson, D. Haskel, Y. Choi, J. Lang, C. Sánchez-Hanke, and B. Hjörvarsson, Phys. Rev. B **90**, 104403 (2014).
[13] S. A. Droulias, G. K. Palsson, H. Palonen, A. Hasan, K. Leifer, V. Kapaklis, B. Hjörvarsson, and M. Wolff, Thin Solid Films **636**, 608 (2017).
[14] R. K. Kawakami, E. J. Escorcia-Aparicio, and Z. Q. Qiu, Phys. Rev. Lett. **77**, 2570 (1996).
[15] A. N. Anisimov, W. Platow, P. Poulopoulos, W. Wisny, M. Farle, K. Baberschke, P. Isberg, B. Hjörvarsson, and R. Wäppling, J. Phys.: Condens. Matter **9**, 10581 (1997).
[16] D. Labergerie, C. Sutter, H. Zabel, and B. Hjörvarsson, J. Magn. Magn. Mater. **192**, 238 (1999).
[17] F. Magnus, M. E. Brooks-Bartlett, R. Moubah, R. A. Procter, G. Andersson, T. P. A. Hase, S. T. Banks, and B. Hjörvarsson, Nat. Commun. **7**, 11931 (2016).